Host-Graft Synapses Form Functional Microstructures and Shape the Host Light Responses After Stem Cell-Derived Retinal Sheet Transplantation

Ryutaro Akiba,[1,2] Hung-Ya Tu,[2,3] Tomoyo Hashiguchi,[2] Yoshiko Takahashi,[2] Kiminori Toyooka,[4] Yoshihiko Tsukamoto,[5] Takayuki Baba,[1] Masayo Takahashi,[2,6] and Michiko Mandai[2,6]

[1]Chiba University Graduate School of Medicine, Department of Ophthalmology, Chuo-ku, Chiba, Japan
[2]RIKEN Center for Biosystems Dynamics Research, Laboratory for Retinal Regeneration, Minato-jima, Chuo-ku, Kobe, Hyogo, Japan
[3]Institute for Protein Research, Osaka University, Suita-shi, Osaka, Japan
[4]RIKEN Center for Sustainable Resource Science, Tsurumi-ku, Yokohama, Kanagawa, Japan
[5]Hyogo Medical University, Department of Biology, Nishinomiya, Hyogo, Japan
[6]Kobe City Eye Hospital Research Center, Minato-jima, Chuo-ku, Kobe, Hyogo, Japan

Correspondence: Michiko Mandai, Research Center, Kobe City Eye Hospital, 2-1-8 Minatojima-minamimachi, Chuo-ku, Kobe, Hyogo 650-0047, Japan; e_lab.mandai@kcho.jp.

Received: July 17, 2024
Accepted: September 15, 2024
Published: October 7, 2024

Citation: Akiba R, Tu HY, Hashiguchi T, et al. Host-graft synapses form functional microstructures and shape the host light responses after stem cell-derived retinal sheet transplantation. *Invest Ophthalmol Vis Sci.* 2024;65(12):8. https://doi.org/10.1167/iovs.65.12.8

Purpose. Retinitis pigmentosa represents a leading cause of blindness in developed countries, yet effective treatments for the disease remain unestablished. Previous studies have demonstrated the potential of stem cell-derived retinal organoid (SC-RO) sheet transplantation to form host-graft synapses and to improve light responsiveness in animal models of retinal degeneration. However, the detailed microstructures of these de novo synapses and their functional contribution have not been well elucidated. This study aims to (1) elucidate the microstructures of the host-graft synapse, and (2) investigate the overall distribution and contribution of these synapses to host retinal light responses.

Methods. We identified host-graft synapses using a reporter system in mouse SC-RO and rd1 mice, a well-established model of end-stage retinal degeneration. Correlative array tomography was used to reveal the microstructure of host-graft synapses. Furthermore, we developed a semi-automated algorithm that robustly detects the host-graft photoreceptor synapses in the overall grafted area using the same reporter system in flat-mount retinas. We then integrated the spatial distribution of the host-graft synapses with light responses detected by multi-electrode array recording.

Results. Correlative array tomography revealed that host-graft synapses recapitulate the developmental process of photoreceptor synapse formation involving horizontal cells first and then rod bipolar cells. By integrating the spatial distribution of host-graft synapse and multi-electrode array recording, we showed that the number of light-responsive host retinal ganglion cells is positively correlated with the local density of host-graft synapses.

Conclusions. De novo host-graft synapses recapitulate the developmental microstructure of the photoreceptor synapse, and their formation contributes to the light responsiveness after SC-RO transplantation.

Keywords: stem cell therapy, retinal degeneration, synaptogenesis, electron microscopy, photoreceptor transplantation

Retinitis pigmentosa (RP) is the second leading cause of vision loss in adulthood in Japan,[1] and predominantly contributes to blindness in developed countries worldwide. RP is characterized by retinal degeneration resulting from a multitude of gene mutations[2] that lead to photoreceptor cell death. Despite the prevalence and influence of RP, there is no established treatment so far. Promising results have been reported in previous studies investigating cell transplantation therapy for RP.[3–6] Embryonic stem (ES) cells[7–10] or induced pluripotent stem (iPS) cells[11–14] can be useful source of photoceptor cells for transplantation. Transplantation of photoreceptor (precursor) cells have been reported to recover visual function in the animal models of retinal degeneration.[15–18] We have also demonstrated that the transplanted mouse stem cell-derived retinal organoid (SC-RO) sheet can integrate into the host retinal network and restore visual function in the end-stage retinal degeneration mice models,[19,20] and also the human SC-RO in primate models of localized retinal degeneration.[21,22] Mandai et al. provided evidence of host-graft synapse formation using reporter graft cell lines expressing genetically labeled synaptic marker and rod bipolar reporter mouse line, combined with synapse marker immunostaining.[19] Further, Matsuyama et al.[23] reported an improved transplantation effect by using

genetically engineered bipolar cell deficient grafts (Islet1$^{-/-}$ and Bhlhb4$^{-/-}$) where the quantitative analysis revealed that greater number of graft photoreceptors form synapses per host rod bipolar cells compared to those in the wildtype graft, while approximately 15% of host rod bipolar cells can form synapses with graft photoreceptors in all genotypes of grafts. With these genetically engineered grafts, visual function was better improved in rd1 mice compared to those transplanted with wildtype grafts. Additionally, Akiba et al.[24] revealed that postoperative light environment affects the formation of photoreceptor synapses following transplantation. These studies assessed the host-graft synapses quantitatively; however, it demands further comprehensive evaluation to understand the functional contribution of the de novo synapses to the visual improvement.

Recently, the presence of a phenomenon called "material transfer" was reported, wherein transplanted photoreceptors transfer proteins to host photoreceptors that potentially contribute to the visual function.[25–27] With a possible visual improvement by any remaining host photoreceptor cells rescued via such material transfer, evaluation of the contribution by host-graft synaptic construction to the functional recovery after transplantation can be obscured. On the other hand, material transfer cannot be observed once the photoreceptors are degenerated. Using the end-stage retinal degeneration model where few host photoreceptor cells remain helps simplify this issue. Furthermore, correlating the distributions of host-graft synapses and the response of host retinal ganglion cells (RGCs) to light will allow the quantitative evaluation of the de novo synapse mediated recovery of host visual function after transplantation.

Another considerable issue is the quality of host-graft synapses in terms of functionality. That is, whether de novo synapses can reconstruct the microstructure similar to the typical photoreceptor synapse in healthy retinas. Photoreceptor ribbon synapses form the triad structure where two horizontal cell processes and one bipolar cell dendrite invaginate into a photoreceptor axonal terminal.[28] Assawachananont et al.[20] and Ribeiro et al.[17] reported that the synaptic ribbons associated with bipolar dendrite invagination were observed within the mouse or human iPS cell-derived photoreceptor transplantation site by transmission electron microscopy (TEM). However, the reported TEM images provided limited clues to identify the individual cells recruited to the host-graft synapse formation.

In the present study, in order to characterize the host-graft synapses, we first examined their microstructures by applying the correlative array tomography technique[29] on semi-thin sections, which allowed us to identify the fluorescence-labeled host bipolar cell and graft synaptic ribbon at the electron microscopy level. We then quantified the de novo synapses using a semi-automatic algorithm to draw the density maps of host-graft synapses in the grafted areas and compared them with the host RGC light responses. We also investigated such synapse-function correlation in the retinas engrafted with wildtype and genetically engineered bipolar cell deficient grafts.

Materials and Methods

Detailed methods for retinal organoid differentiation, transplantation, correlative array tomography, multielectrode array (MEA) recordings, immunostaining, and synapse counting are provided in the Supplementary Information. All animal experiments were conducted with accordance to ARVO Statement for the Use of Animals in Ophthalmic and Vision Research.

Results

Identification of Photoreceptor-Bipolar Cell Synapse by Correlative Array Tomography

First, we examined whether the correlative array tomography is useful upon identifying the photoreceptor synapses in the control retina of L7-GFP mouse in which the rod bipolar cells are labeled with GFP (see the Supplementary Information for detailed histological procedures). Using 50-µm-thick sections, we immunostained the photoreceptor ribbon with an anti-CtBP2 antibody and then stained it with DAPI for visualization of cell nuclei (Fig. 1A). Confocal images showed multiple photoreceptor synapses where rod bipolar cells extended their dendrites toward photoreceptor ribbons. Samples were then post-fixed, stained en bloc, dehydrated, and then embedded in resin for cutting. We stained 500-nm serial sections with toluidine blue (TB) to identify the region of interest (ROI) by the rosette structure composed of photoreceptor nuclei (Fig. 1B). A field emission scanning electron microscopy (FE-SEM) image of the corresponding area was also obtained using the YAG-BSE detector and the correlative light and electron microscopy system[29] (Fig. 1C). The fluorescence, TB staining, and FE-SEM images were superimposed based on the spatial arrangement of photoreceptor nuclei (Fig. 1D). We then took the high-magnification FE-SEM images at two photoreceptor synapses (Figs. 1A–D, white box), as shown in the yellow and blue boxes in Figure 1E with ribbons indicated by white arrowheads. The ribbons overlapped with the confocal images of CtBP2 signals (red) and opposed the invaginating bipolar cell process (green).

Further magnification of the photoreceptor synapse at the yellow and blue boxes of Figure 1E shows the typical triad structure of the photoreceptor synapse constituted by two horizontal cell processes (H) and one invaginating bipolar cell process (B), opposing the synaptic ribbon (arrowhead in (Figs. 1F, 1G). The ribbon is an electron-dense lamella typically located just above an evaginated ridge of the presynaptic membrane. Two electron-dense microstructures can be recognized at high magnification to assess the maturation of ribbons and H and B processes. One is a curved dense band called "arciform density," which exists between the ribbon and the presynaptic membrane for anchoring the ribbon to the ridge membrane.[30] McLaughlin and Reese[31] reported that this microstructure matures as the photoreceptor synapse develops. We observed the arciform density in our FE-SEM (Figs. 1F, 1G, white circle). The other microstructure is a submembrane dense band called "fluffy density," which extends along the photoreceptor cell membrane that faces the postsynaptic mGluR6 receptors and possibly other related synaptic molecules on the invaginating ON bipolar cell dendrites.[32] Fluffy density is observed where the dystrophin-glycoprotein complex links the cytoskeleton and membrane-associated proteins to the extracellular matrix for organizing the trans-synaptic signaling system,[33] and Ueda et al.[34] demonstrated dystrophin immunoreactivity coinciding with the fluffy density region, which borders the rod bipolar invaginating dendrites but not the horizontal cell processes. We also found the fluffy density in our FE-SEM as indicated by yellow arrows in Figures 1F and 1G. In addition, by immunohistology we often observed the presence of

Investigative Ophthalmology & Visual Science

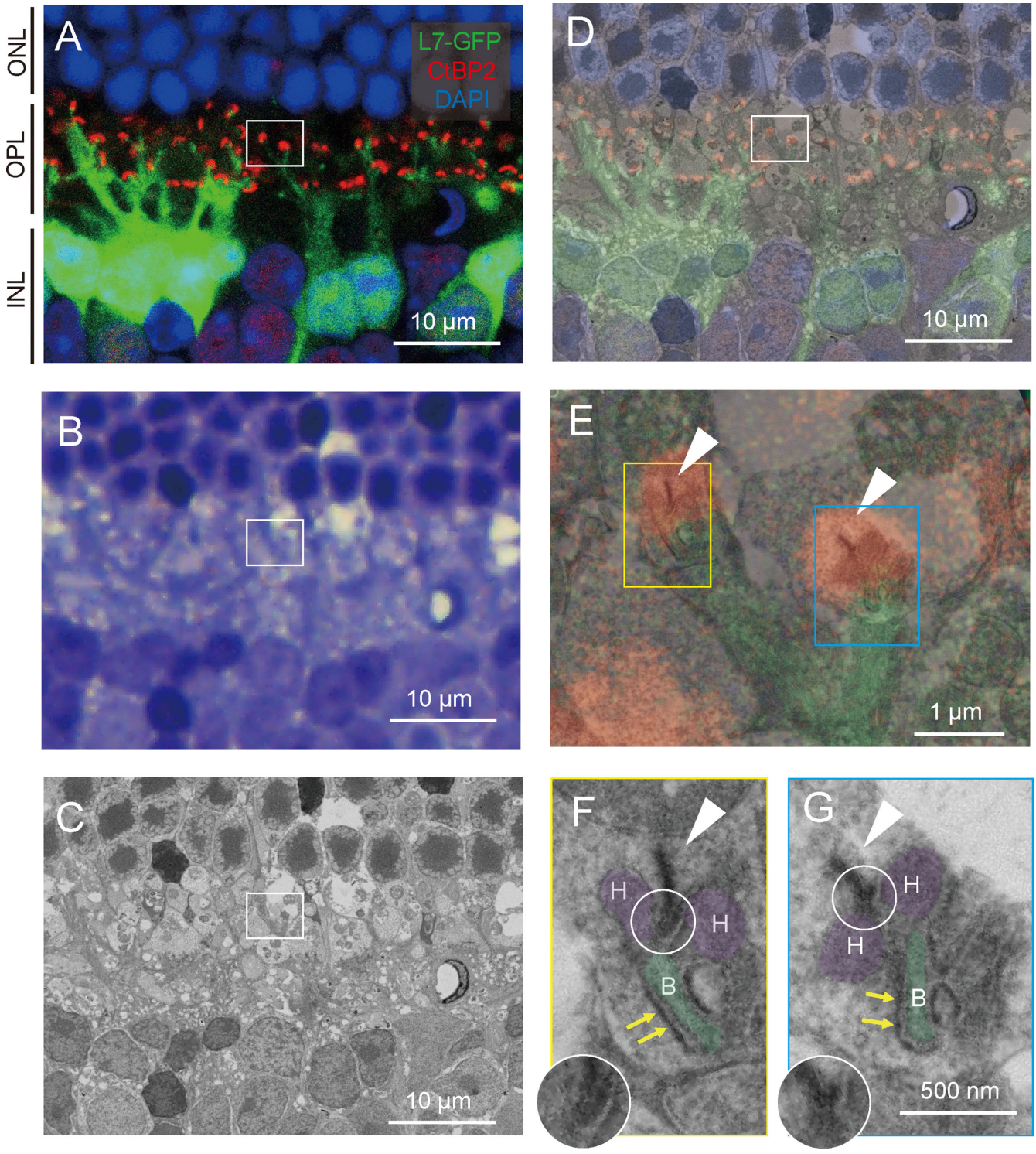

Figure 1. Correlative array tomography images of control retina. (**A**) Confocal microscopy image of L7-GFP+ rod bipolar extending their dendrites toward photoreceptor's synaptic ribbon (CtBP2-tdTomato). *Green* = L7-GFP; *red* = CtBP2-tdTomato; and *blue* = DAPI. INL, inner nuclear layer; OPL, outer plexiform layer; ONL, outer nuclear layer. (**B**) Toluidine blue staining image corresponding to the **A** panel. (**C**) Field emission scanning electron microscopy (FE-SEM) image corresponding to the **A** panel. (**D**) Overlayed image of the **A** and **B** panels. (**E**) Magnified image of photoreceptor synapses indicated by the *red box* in the **D** panel. Synaptic ribbons are indicated by *white arrowheads*. (**F, G**) High magnification of FE-SEM image of photoreceptor synapse showing triad structure. Synaptic ribbons are indicated by *white arrowheads*, arciform densities by *white circles*, and fluffy densities by *yellow arrows*. Horizontal cell processes ("H") are colored *purple*, and rod bipolar cell processes ("B") are colored *green*. The arciform density is magnified without pseudocolor as inset in the **F** and **G** panels.

Investigative Ophthalmology & Visual Science

mGluR6 signals at the contact site of host bipolar dendrites and graft photoreceptors, as detailed in the latter half of this paper (Supplementary Fig. S2). These observations confirm that correlative array tomography is useful in identifying the photoreceptor synapses with multimodal imaging techniques.

Host-Graft Junctions Form Characteristic Microstructures of Photoreceptor Synapse

Next, we transplanted mouse embryonic stem cell-derived retinal organoids to the subretinal space of degenerated rd1 host mice as the host. Rd1 is a commonly used mouse model of progressive retinal degeneration in which photoreceptor cells degenerate rapidly, with most cells lost in the first 4 weeks after birth. The graft rod photoreceptors' synaptic ribbons were genetically labeled with CtBP2-tdTomato expression under Nrl promoter, whereas the host rod bipolar cells were GFP-positive driven by L7 promoter. Those fluorescence images were superimposed on FE-SEM images to analyze the target host-graft synapses at the ultrastructural level. We examined the ultrastructure of host-graft interfaces by correlating the fluorescence image with the FE-SEM image of our ROI where host-graft synapse formation was observed.

Although the host rd1 mouse was 20 weeks old at the time of transplantation, the host rod bipolar cells were observed extending their dendrites to reach graft photoreceptors as shown in Figures 2A, 2D, and 2G. Within each white box there were CtBP2-tdTomato signals. The CtBP2-tdTomato signals in the confocal images (red signal in Figs. 2B, 2E, 2H) overlapped with synaptic ribbons in the corresponding FE-SEM images (white arrowheads

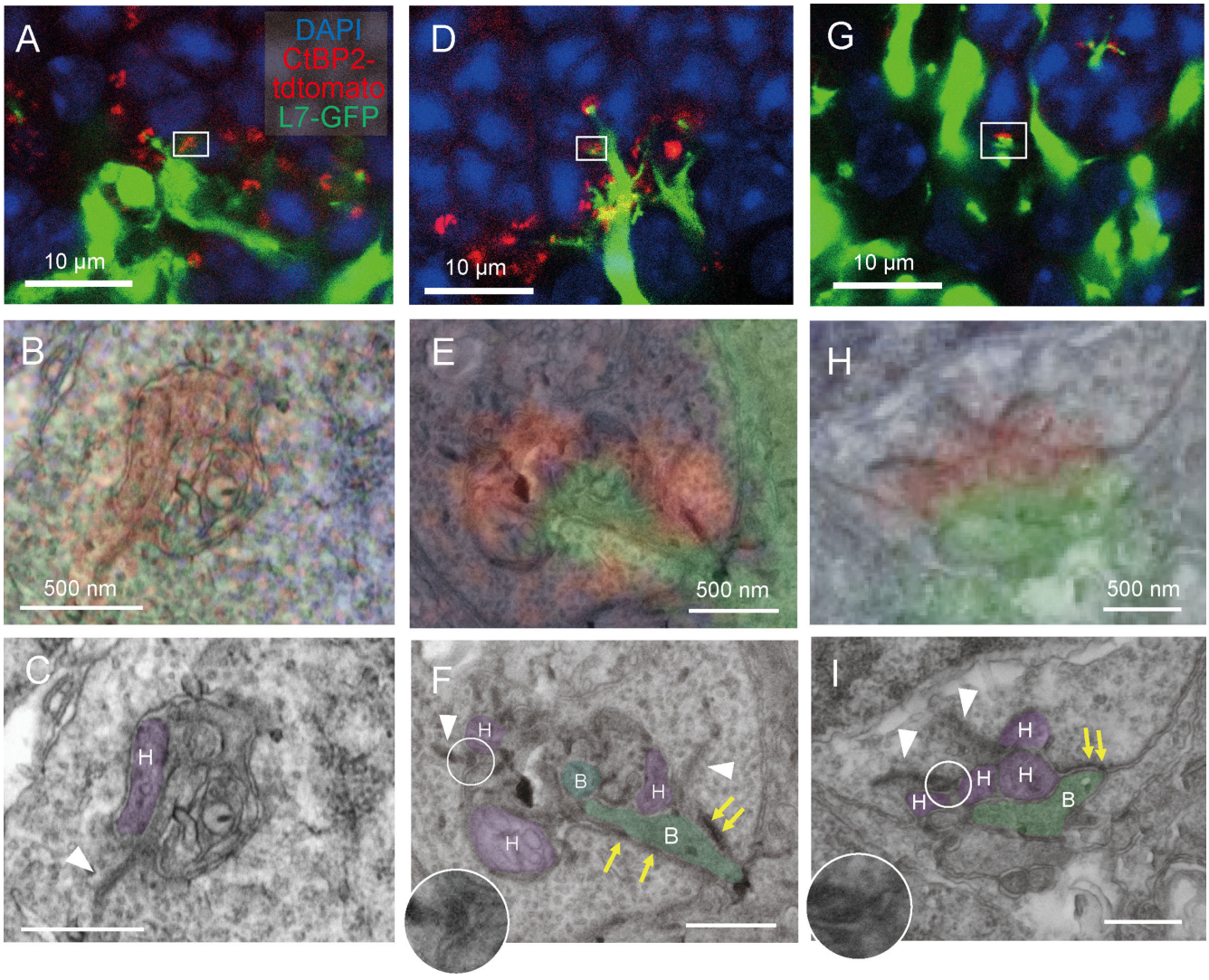

Figure 2. Correlative array tomography images of host-graft synapse after retinal organoid transplantation. (**A**) Confocal microscopy image of the host-graft synapse after wildtype mouse stem cell-derived retinal organoid. *Green* = L7-GFP, *red* = CtBP2-tdTomato, and *blue* = DAPI. (**B**) High magnification image of the confocal image corresponding to the *white box* in panel **A** with the field emission scanning electron microscopy (FE-SEM) images superimposed. (**C**) FE-SEM image of panel **B**. Processes of horizontal cells are colored in *purple* and labeled with "H." (**D–F, G–I**) Examples from other host-graft synapses identified by the correlative array tomography. Horizontal cell processes ("H") are colored *purple*, and rod bipolar cell processes ("B") are colored *green*. Synaptic ribbons are indicated by *white arrowheads*, arciform densities by *white circles*, and fluffy densities by *yellow arrows*. The arciform density is magnified without pseudocolor as inset in the **F** and **I** panels.

Investigative Ophthalmology & Visual Science

in Figs. 2C, 2F, 2I). The presence of arciform densities (white circles in Figs. 2F, 2I) associated with the ribbon was also confirmed.

In contrast, the GFP signals of the host rod bipolar cells were considerably variable depending on individual host-graft synapses even at the adjacent location. The rod terminal synaptic cavity was occasionally packed by multiple meandering processes, as shown in Figures 2B and 2C. However, we had limited observational data to identify the cell types from which these processes were derived. The absence of a GFP signal or bipolar synaptic microstructures suggested the lack of invagination by the host rod bipolar cells. Nevertheless, we found a possible horizontal cell process as the lateral element of the ribbon synapse according to the well-known structural evidence (see Fig. 2C, purple process with "H" label). Another host-graft synapse showed a stronger GFP signal expressed by the host rod bipolar cell (see Fig. 2D), and the high magnification image showed the GFP signal (see Fig. 2E) overlapping with the invaginating rod bipolar cell process in the corresponding FE-SEM image (see Fig. 2F, green process with "B" label). The arciform density (white circle) at the base of the synaptic ribbon and the fluffy density (yellow arrows) at the photoreceptor membrane opposing the bipolar cell process were found in this particular synapse, suggesting relative maturation compared to that in Figures 2A to 2C.

Another host-graft synapse (Figs. 2G, 2H) exhibited multiple ribbons with arciform density at each ribbon base. This synapse also had shallow invagination of bipolar cell process, accompanied by presynaptic fluffy density at the opposing membrane of the rod spherule (see Fig. 2I). We also found host-graft synapses (Supplementary Fig. S1A–S1C) that resemble typical triad synapses observed in the control retina (see Fig. 1F) with two lateral horizontal cell processes alongside the synaptic ribbon and the invaginating host rod bipolar cell process (see Supplementary Fig. S1C).

These results indicate that host-graft photoreceptor synapses identified by the genetic labeling of L7-GFP and CtBP2-tdTomato are capable of developing synaptic microstructures similar to normal photoreceptor synapses, with preceding horizontal cell invagination followed by invagination of the host bipolar cell processes toward the host synaptic ribbon.[35]

Spatial Distributional Mapping of Host-Graft Synapses Using Semi-Automated Synapse Quantification

We previously reported an automated 2D approach for photoreceptor synapse quantification[24] and a manual 3D host-graft synapse quantification on reconstructed confocal images.[23] In the present study, we further refined these approaches to establish an efficient and robust semi-automated 3D synapse quantification protocol by incorporating multiple tools from Imaris software. The host-graft synapses labeled by fluorescent reporter markers and immunostaining were semi-automatically distinguished from the confocal images of flat-mount retinas after MEA recordings, and their spatial distribution was mapped along with the recorded RGC activities. The correlation between synapse distribution and host RGC responses was then examined. In addition to the wildtype graft, we transplanted the genetically engineered grafts with a reduced number of graft bipolar cells,[23] to examine whether the reduction of the bipolar cells may affect the relationship between host-graft synapse formation and the light responses from host RGCs.

Photoreceptor synapses were identified as the colocalized pre-synaptic marker CtBP2-tdTomato expressed by graft photoreceptors and post-synaptic marker mGluR6 on L7-GFP host rod bipolar cell dendritic tips. To quantify these synapses, we utilized the "Spots" function in Imaris to determine the center coordinates of the pre-synaptic CtBP2-tdTomato signals (see Supplementary Figs. S2A, S2B). After creating a 3D mask for the GFP-positive bipolar cells using the "Surface" function (see Supplementary Fig. S2C), we used the "Spots" function again to determine the coordinates of the post-synaptic marker mGluR6 within the L7-GFP signals (see Supplementary Figs. S2D, S2E). Finally, the "coloc" analysis was executed to identify pre- and post-synaptic signals that colocalized within 1-µm range to distinguish the host-graft synapses (see Supplementary Fig. S2F). An example of host-graft synapse quantification after transplantation of Bhlhb4$^{-/-}$ graft is shown in Figures 3A to 3C. The mGluR6 signals were detected at the tips of the host rod bipolar cell dendrites (see Fig. 3A); when the CtBP2-tdTomato signals were detected opposed to these dendrites (see Fig. 3B), it was defined as a host-graft synapse by our method (see Fig. 3C). High magnification of a detected host-graft synapse (indicated by the white box in Figs. 3A–3C) showed colocalization of graft CtBP2-tdTomato and mGluR6 signals at the tip of host rod bipolar cell (see Figs. 3D, 3F). In the CtBP2-tdTomato channel of the flat-mount view, we observed the characteristic rosette structure of graft photoreceptor cells (see Fig. 3K) that largely overlapped with the detected host-graft synapses (see Fig. 3L). Photoreceptor rosette structures were similarly observed in transplantation with wildtype (see Fig. 3G) and Islet1$^{-/-}$ (see Fig. 3I) grafts, and the host-graft synapses were similarly formed in those samples (se Figs. 3H, 3J).

Synapse Coordinates and Electrophysiological Responses

Next, we investigated whether the distribution of host-graft synapses related with the light-driven activities of host RGCs recorded by MEA. Representative examples were shown to demonstrate the synapse-function correlation for wildtype (Figs. 4A–C), Islet1$^{-/-}$ (Figs. 4D–F), and Bhlhb4$^{-/-}$ (Figs. 4G–I) grafts. To align the coordinates of MEA electrodes and host-graft synapses, we utilized the infrared DIC image with tdTomato fluorescence captured after MEA recordings and the immunofluorescence image. Precise alignment was achieved by matching the rosette structure of the graft in both images (see Figs. 4A, 4D, 4G), and the X-Y coordinates of the host-graft synapses were plotted along with the corresponding MEA electrodes, together with the number of light responsive RGCs detected at each electrode (see Figs. 4B, 4E, 4H). The size of the magenta circles reflects the number of light-responsive RGCs and tends to be larger where the host-graft synapses were densely detected.

For statistical analysis, Spearman's rank correlation test was used to evaluate the association between the number of host-graft synapses at a specific distance from an individual electrode and the number of light responsive RGCs detected by that electrode. The correlative coefficients between synapse and cell numbers were calculated for every 50-µm radial bin from the electrode at a 25-µm step size

Investigative Ophthalmology & Visual Science

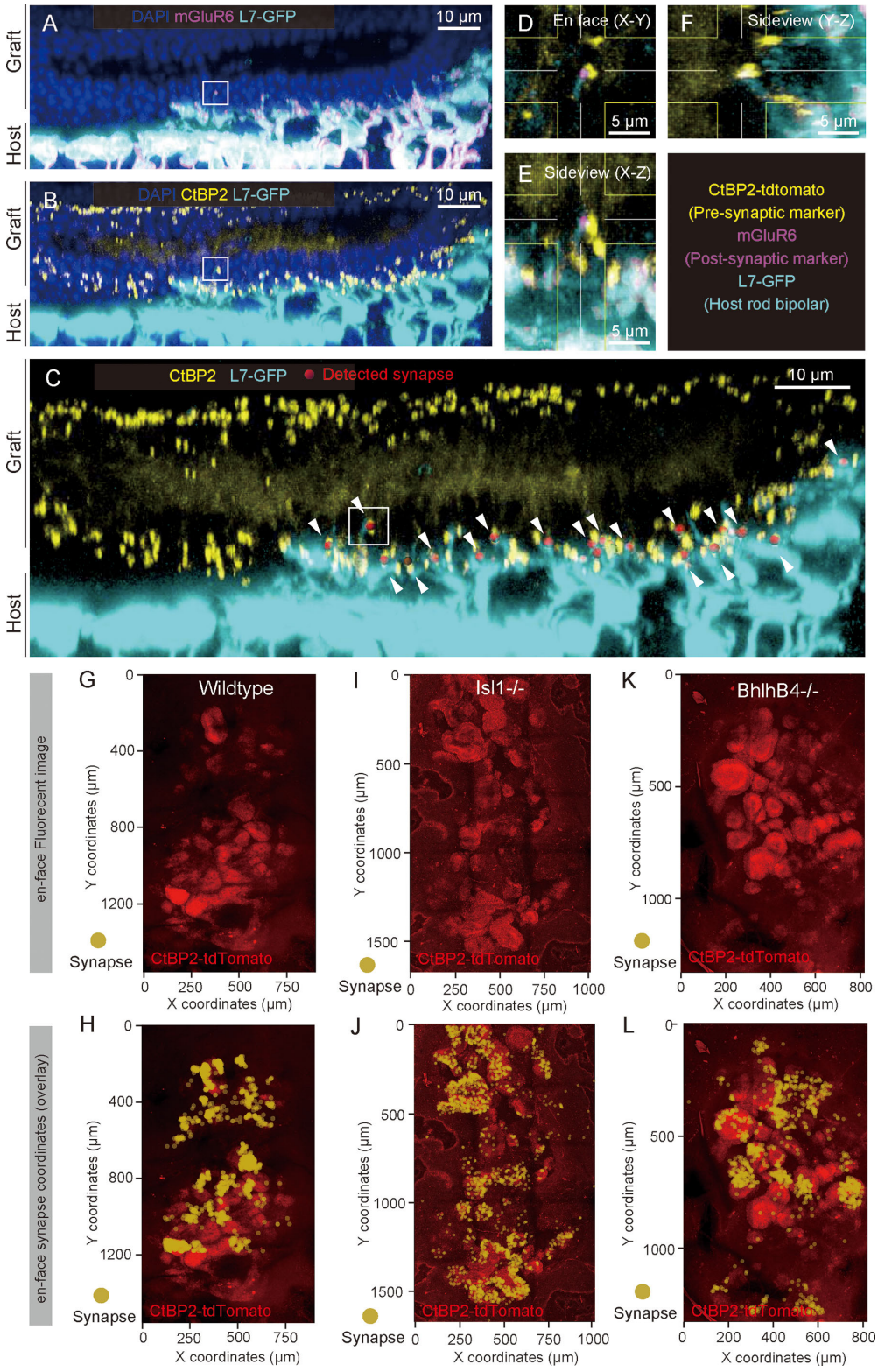

Figure 3. Examples of Semi-automated 3D quantification of host-graft synapse. (**A**) Confocal image of host-graft synapse used for semi-automated host-graft synapse quantification (Bhlhb4$^{-/-}$ graft). The mGluR6 signals colocalize with the tips of host rod bipolar cell dendrites extending toward the transplanted photoreceptor cells. (**B**) Host rod bipolar cells extending dendrites toward graft photoreceptor's synaptic ribbon (CtBP2). (**C**) Host-graft synapses identified by co-localization of pre-synaptic marker (CtBP2), post-synaptic marker (mGluR6), and host-rod bipolar cell (L7-GFP; *white arrowheads*). (**D–F**) Magnified orthogonal view of the detected host-graft synapse in the white box in panels **A** to **C**. Post-synaptic marker mGLuR6 (*magenta*) was expressed at the host rod bipolar cell dendritic tip, which colocalized with pre-synaptic marker CtBP2 (*yellow*). (**G–L**) Example of flat-mount confocal image in CtBP2 channel of rd1 retina after transplantation of wildtype (**G, H**), Islet1$^{-/-}$ (**I, J**), and Bhlhb4$^{-/-}$ (**K, L**) grafts and MEA recording. Coordinates of detected host-graft synapse are indicated by *yellow dots* as shown in panels **H**, **J**, and **L** and overlayed to each flat-mount image of the red CtBP2 channel.

Investigative Ophthalmology & Visual Science

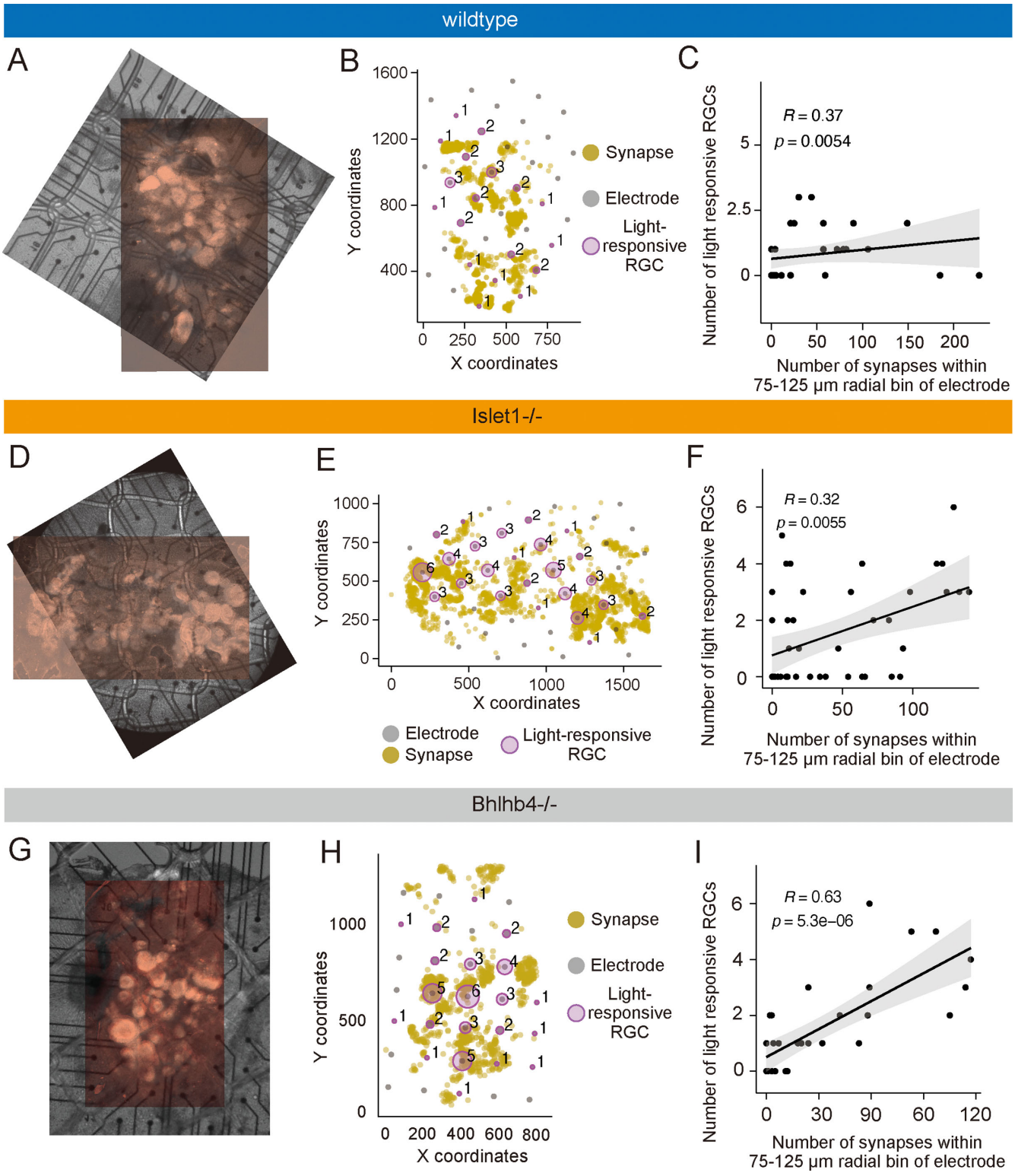

Figure 4. Host-graft synapse coordinates and multielectrode array (MEA) recording results. (**A**) Flat-mount confocal image of retina transplanted with wildtype graft, aligned and overlayed with the infrared image with tdTomato fluorescence taken after MEA recording. (**B**) Coordinates of host-graft synapse (*yellow dots*) and MEA electrodes (*gray dots*). The numbers of light-responsive host retinal ganglion cells (RGCs) were represented with the radius of the *magenta circle* with the number alongside. (**C**) Result of Spearman's rank correlation test between host-graft synapse numbers within 75 to 125 µm radial bin of MEA electrode and the number of light responsive RGC numbers detected by that electrode after wildtype graft transplantation. (**D–F**) Equivalent result to panels **A** to **C** obtained after Islet1$^{-/-}$ transplantation. (**G–I**) Equivalent result to panels **A** to **C** obtained after Bhlhb4$^{-/-}$ transplantation.

Investigative Ophthalmology & Visual Science

(Supplementary Fig. S4A), and averages at each distance were regressed by the "locally estimated scattered smoothing" method to identify the peak of mean correlative coefficients (see Supplementary Fig. S4B). For all three types of grafts, we found peaks of correlation at around 100 µm ± 25 µm distance, suggesting host-graft synapses distributed at this distance from the detected RGCs contributed the most to their light responses. Examples of correlation plot of samples from wildtype, Islet1$^{-/-}$, and Bhlhb4$^{-/-}$ grafts are shown in Figures 4C, 4F, and 4I, respectively. All 3 samples showed positive and statistically significant correlations between the host-graft synapse numbers within 100 ± 25 µm radial bin and the number of light-responsive RGCs on the corresponding electrodes (see Figs. 4C, 4F, 4I). Results of the other samples were shown in Supplementary Figure S5 with a similar trend, except for one sample transplanted with wildtype graft that had no light-responsive RGCs detected despite the presence of host-graft synapses (see Supplementary Figs. S5G–S5I). In contrast, Islet1$^{-/-}$ and Bhlhb4$^{-/-}$ grafts showed more robust relationship between the synapse density and the light-responsive RGC numbers (see Supplementary Fig. S4C). Although the number of samples is limited, our findings denote the host-graft synapse contribution to the recovery of local retinal light responsiveness. In addition, the genetically engineered grafts might lead to more robust structure-function relationship of the host-graft synapse, which will be better clarified in future studies with larger sample numbers.

Discussion

In the current study, we aimed to shed light on the qualitative features of de novo host-graft synapses and the relevance of their quantitative features to the functional circuitry reconstruction following mouse SC-RO transplantation. For this purpose, we examined the microstructures of host-graft synapses using the correlative array tomography technique and developed an efficient protocol to correlate the spatial distribution of overall host-graft synapses and of host RGC light responses.

With the reporter system in which host rod bipolar cells and graft photoreceptor synaptic protein CtBP2 were robustly labeled with fluorescence, we could readily identify the host-graft synaptic contacts. By adopting the correlative array tomography technique, we were able to examine the ultrastructure of host-graft synapses in detail, and to confirm the presence of functional synaptic component and the involvement of horizontal cells at the synapses which were clearly identified by reporter marker colocalization.

Past electron microscopy studies reported the presence of "fluffy density" on the photoreceptor cell membrane that is opposed to the mGluR6 receptor of the ON bipolar cells,[32] and this observation was useful to distinguish the rod bipolar cell processes that could be confirmed by the GFP expression of the host rod bipolar cells in the present study. Interestingly, in addition to the typical triad synapses resembling those in the control retina (see Supplementary Figs. S1A–S1C), we also observed unconventional motifs of the photoreceptor synapses including the ones with only the horizontal cell invagination (see Figs. 2A–2C), atypical (non-triad) synapse yet consisting horizontal cell and bipolar cell invagination with fluffy densities (see Figs. 2D–2F), and immature synapses with shallow invagination of bipolar cells (see Figs. 2G–2I). These synapses seem to recapitulate the developmental process of the photoreceptor synapse where the horizontal cells innervate first, followed by the invagination of the bipolar cells.[33,35] In line with the observation, we did not identify any host-graft synapses with only the host bipolar cell innervation.

Because our retinal organoid grafts contain horizontal cells,[23] at this moment, it is not clear whether horizontal cells in these synaptic triads originate from host or graft. Horizontal cells are known to contribute to various early visual processing, for example, forming center-surround receptive field that enhances the spatial discrimination, the post-receptoral light adaptation, and the generation of color opponency.[36] Because invagination of horizontal cells is reported to precede that of bipolar cells,[33,35] neighboring graft horizontal cells in the same developmental stage with graft photoreceptor cells may also take the first action in the formation of host-graft synapses. Knowing which and how horizontal cells may initiate the de novo synapse formation would be important to facilitate the functional integration of graft photoreceptors. Future experiments incorporating the serial section imaging techniques to trace individual cells involved in the host-graft synapses will lead to a more comprehensive analysis of the connectomes underlying host-graft synaptogenesis. Factors that further facilitate synapse maturation and/or synaptic integration would also be the key to enhance the functional recovery after graft transplantation.

Previous studies have suggested that transplanted photoreceptors could transfer proteins to host photoreceptors, leading to "material transfer" as a potential explanation for functional improvements.[25–27] To reduce such confounding factors, we used 8 to 13 week old rd1 mice for transplantation, whose rod photoreceptors degenerate prior to the cone photoreceptor loss and therefore leaving few if any photoreceptor cells remain.[37] We conducted MEA recordings 8 to 12 weeks after transplantation (mice up to 21 weeks of age) and found RGCs on and near the grafted areas responded robustly to light stimulation within the mesopic range, indicating that the functional synaptic connections formed between graft and host retinal cells. Our electron microscopic observation in the current study further supported the presence of functional host-graft synapses that may well contribute to the restoration of local retinal light responsiveness.

Moreover, we developed a semi-automated, fluorescent image-based algorithm to efficiently quantify the host-graft synapses. This protocol enabled us to demonstrate the overall distribution of possible host-graft transmission sites over the grafted area. We previously adapted the similar approach with manual counting to show that photoreceptor cells in grafts with reduced bipolar cell numbers form more synapses with host bipolar cells.[23] In the current study, by generating the density map of host-graft synapses over the grafted area, we were able to evaluate the synapse density and local host RGC responses altogether. Although this protocol does not fully characterize synaptic quality in detail to discriminate the atypical and/or immature synapses seen in our electron microscopic (EM) observation, it does reveal the potential synaptic transmission sites. The positive correlation between the number of host-graft synapses and light responsive host retinal ganglion cells implies the significance of these host-graft synapses in retinal cell therapy. Although the sample number was limited, genetically modified grafts with reduced bipolar cells showed more robust correlation between the host-graft synapse number and host RGC responses. This suggests that the graft-origin

Investigative Ophthalmology & Visual Science

bipolar cells compete with the host bipolar cells for photoreceptor synaptic contacts, and by depleting the graft-origin bipolar cell partners, functional synapse formation of graft photoreceptors with host bipolar cells may be enhanced. In addition, further analysis of how host or graft horizontal cells contribute to host-graft synapse formation, and the process of how each cell type is recruited, will provide clues for future regenerative therapeutic approaches to improve host-graft synaptic formation and the subsequent functional recovery as an immediate priority.

Acknowledgments

Supported by JSPS KAKENHI Grant Number JP19K09942, and AMED Grant Number JP20bm0204002.

Further information and requests for resources and reagents should be directed to and will be fulfilled by the corresponding author Michiko Mandai (michiko_mandai@kcho.jp).

Author Contributions: Conception and design, financial support: M.M. Data acquisition: R.A., H.-Y.T., T.H., Y. Ta., and K.T. Data analysis and interpretation: R.A., H.-Y.T., M.M., Y.Ts., T.B., and M.T. Manuscript writing: R.A., H.-Y.T., Y.Ts., and M.M. The final manuscript was approved by all the authors.

Disclosure: **R. Akiba**, None; **H.-Y. Tu**, None; **T. Hashiguchi**, None; **Y. Takahashi**, None; **K. Toyooka**, None; **Y. Tsukamoto**, None; **T. Baba**, None; **M. Takahashi**, None; **M. Mandai**, patent "WO2018/097253" regarding the genetically engineered retinal organoid

References

1. Morizane Y, Morimoto N, Fujiwara A, et al. Incidence and causes of visual impairment in Japan: the first nation-wide complete enumeration survey of newly certified visually impaired individuals. *Jpn J Ophthalmol*. 2019;63:26–33.
2. Schneider N, Sundaresan Y, Gopalakrishnan P, et al. Inherited retinal diseases: linking genes, disease-causing variants, and relevant therapeutic modalities. *Prog Retin Eye Res*. 2022;89:101029.
3. MacLaren RE, Pearson RA, MacNeil A, et al. Retinal repair by transplantation of photoreceptor precursors. *Nature*. 2006;444:203–207.
4. Barber AC, Hippert C, Duran Y, et al. Repair of the degenerate retina by photoreceptor transplantation. *Proc Natl Acad Sci USA*. 2013;110:354–359.
5. Gonzalez-Cordero A, West EL, Pearson RA, et al. Photoreceptor precursors derived from three-dimensional embryonic stem cell cultures integrate and mature within adult degenerate retina. *Nat Biotechnol*. 2013;31:741–747.
6. Van Gelder RN, Chiang MF, Dyer MA, et al. Regenerative and restorative medicine for eye disease. *Nat Med*. 2022;28:1149–1156.
7. Osakada F, Ikeda H, Mandai M, et al. Toward the generation of rod and cone photoreceptors from mouse, monkey and human embryonic stem cells. *Nat Biotechnol*. 2008;26:215–224.
8. Eiraku M, Takata N, Ishibashi H, et al. Self-organizing optic-cup morphogenesis in three-dimensional culture. *Nature*. 2011;472:51–56.
9. Nakano T, Ando S, Takata N, et al. Self-formation of optic cups and storable stratified neural retina from human ESCs. *Cell Stem Cell*. 2012;10:771–785.
10. Gonzalez-Cordero A, West EL, Pearson RA, et al. Photoreceptor precursors derived from three-dimensional embryonic stem cell cultures integrate and mature within adult degenerate retina. *Nat Biotechnol*. 2013;31:741–747.
11. Gonzalez-Cordero A, Kruczek K, Naeem A, et al. Recapitulation of human retinal development from human pluripotent stem cells generates transplantable populations of cone photoreceptors. *Stem Cell Reports*. 2017;9:820–837.
12. Kruczek K, Gonzalez-Cordero A, Goh D, et al. Differentiation and transplantation of embryonic stem cell-derived cone photoreceptors into a mouse model of end-stage retinal degeneration. *Stem Cell Reports*. 2017;8:1659–1674.
13. Meyer JS, Howden SE, Wallace KA, et al. Optic vesicle-like structures derived from human pluripotent stem cells facilitate a customized approach to retinal disease treatment. *Stem Cells*. 2011;29:1206–1218.
14. Zhong X, Gutierrez C, Xue T, et al. Generation of three-dimensional retinal tissue with functional photoreceptors from human iPSCs. *Nat Commun*. 2014;5:4047.
15. Pearson RA, Barber AC, Rizzi M, et al. Restoration of vision after transplantation of photoreceptors. *Nature*. 2012;485:99–103.
16. Lamba DA, Gust J, Reh TA. Transplantation of human embryonic stem cell-derived photoreceptors restores some visual function in Crx-deficient mice. *Cell Stem Cell*. 2009;4:73–79.
17. Ribeiro J, Procyk CA, West EL, et al. Restoration of visual function in advanced disease after transplantation of purified human pluripotent stem cell-derived cone photoreceptors. *Cell Rep*. 2021;35:109022.
18. Gasparini SJ, Tessmer K, Reh M, et al. Transplanted human cones incorporate into the retina and function in a murine cone degeneration model. *J Clin Invest*. 2022;132:e154619.
19. Mandai M, Fujii M, Hashiguchi T, et al. iPSC-derived retina transplants improve vision in rd1 end-stage retinal-degeneration mice. *Stem Cell Reports*. 2017;8:69–83.
20. Assawachananont J, Mandai M, Okamoto S, et al. Transplantation of embryonic and induced pluripotent stem cell-derived 3D retinal sheets into retinal degenerative mice. *Stem Cell Reports*. 2014;2:662–674.
21. Shirai H, Mandai M, Matsushita K, et al. Transplantation of human embryonic stem cell-derived retinal tissue in two primate models of retinal degeneration. *Proc Natl Acad Sci USA* 2016;113:E81–E90.
22. Tu HY, Watanabe T, Shirai H, et al. Medium- to long-term survival and functional examination of human iPSC-derived retinas in rat and primate models of retinal degeneration. *EBioMedicine*. 2019;39:562–574.
23. Matsuyama T, Tu HY, Sun J, et al. Genetically engineered stem cell-derived retinal grafts for improved retinal reconstruction after transplantation. *iScience*. 2021;24:102866.
24. Akiba R, Matsuyama T, Tu HY, et al. Quantitative and qualitative evaluation of photoreceptor synapses in developing, degenerating and regenerating retinas. *Front Cell Neurosci*. 2019;13:16.
25. Pearson RA, Gonzalez-Cordero A, West EL, et al. Donor and host photoreceptors engage in material transfer following transplantation of post-mitotic photoreceptor precursors. *Nat Commun*. 2016;7:13029.
26. Santos-Ferreira T, Llonch S, Borsch O, Postel K, Haas J, Ader M. Retinal transplantation of photoreceptors results in donor-host cytoplasmic exchange. *Nat Commun*. 2016;7:13028.
27. Singh MS, Balmer J, Barnard AR, et al. Transplanted photoreceptor precursors transfer proteins to host photoreceptors by a mechanism of cytoplasmic fusion. *Nat Commun*. 2016;7:13537.
28. Kolb H. Organization of the outer plexiform layer of the primate retina: electron microscopy of Golgi-impregnated cells. *Philos Trans R Soc Lond B Biol Sci*. 1970;258:261–283.

29. Toyooka K, Shinozaki-Narikawa N. Efficient fluorescence recovery using antifade reagents in correlative light and electron microscopy. *Microscopy (Oxf)*. 2019;68:417–421.
30. Schmitz F. Presynaptic [Ca(2+)] and GCAPs: aspects on the structure and function of photoreceptor ribbon synapses. *Front Mol Neurosci*. 2014;7:3.
31. McLaughlin BJ, Reese TS. A freeze-fracture study of photoreceptor presynaptic membranes during ribbon synapse formation. *J Neurocytol*. 1981;10:183–199.
32. Vardi N, Duvoisin R, Wu G, Sterling P. Localization of mGluR6 to dendrites of ON bipolar cells in primate retina. *J Comp Neurol*. 2000;423:402–412.
33. Burger CA, Jiang D, Mackin RD, Samuel MA. Development and maintenance of vision's first synapse. *Dev Biol*. 2021;476:218–239.
34. Ueda H, Baba T, Terada N, Kato Y, Tsukahara S, Ohno S. Dystrophin in rod spherules; submembranous dense regions facing bipolar cell processes. *Histochem Cell Biol*. 1997;108:243–248.
35. Nemitz L, Dedek K, Janssen-Bienhold U. Rod bipolar cells require horizontal cells for invagination into the terminals of rod photoreceptors. *Front Cell Neurosci*. 2019;13:423.
36. Thoreson WB, Mangel SC. Lateral interactions in the outer retina. *Prog Retin Eye Res*. 2012;31:407–441.
37. Fujii M, Sunagawa GA, Kondo M, Takahashi M, Mandai M. Evaluation of micro electroretinograms recorded with multiple electrode array to assess focal retinal function. *Sci Rep*. 2016;6:30719.

Investigative Ophthalmology & Visual Science